DOI: 10.1002/ejoc.200700216

DFT Study on the Sn^{II}-Catalyzed Diastereoselective Synthesis of Tetrahydrofuran from D–A Cyclopropane and Benzaldehyde

Jinsheng Zhang,[a] Wei Shen,[b] and Ming Li*[b]

Keywords: Density functional calculations / Tin / Donor–acceptor systems / Synthesis / Cycloaddition

By means of density functional theory (DFT), the regio- and diastereoselective mechanism for the synthesis of 2,5-disubstituted tetrahydrofuran from a donor–acceptor (D–A) cyclopropane cycloaddition reaction with benzaldehyde catalyzed by $Sn(OTf)_2$ was investigated. As demonstrated, the overall reaction includes the activation of the D–A cyclopropane (*S*)-**1**, an unusual S_N2 attack on the activated cyclopropane, the formation of the tetrahydrofuran coordination complex and the regeneration of the catalyst. The D–A cyclopropane is activated by its combination with $Sn(OTf)_2$, which leads to a decrease in the natural bond orbital (NBO) energy of $\sigma^*_{(C1–C2)}$ and an increase in the dipole moment and angular deviation of the bent bond $\sigma_{(C1–C2)}$. Two nucleophilic reactions generates two chiral carbon centres, and the first one is rate controlling. In the S_N2 reaction, one molecule of trifluoromethane sulfonate forms a hydrogen-bond $H_{(CHO)}\cdots O_{(OTf)}$, which can control the stretching direction of the benzaldehyde. On the whole, the solvation energies of the species increase with increases in the molecular dipole moments, and the solvent effects increase the reaction barriers. The theoretically predicted dominant product is *cis*-(2*R*,5*R*)-tetrahydrofuran. So these can satisfactorily account for the experimental observations.

Introduction

The regiospecificity and stereochemistry of electrophilic carbon–carbon bond cleavage in cyclopropanes have been the subject of considerable investigation and speculation. In particular, donor-acceptor (D–A) cyclopropanes have been studied owing to their easy synthesis and high reactivity, and they are exceptionally useful three-atom building blocks. By employing ligand control to effect absolute stereochemical induction, a series of stereoselective cycloaddition reactions were developed.[1–5] Recently, Pohlhaus et al. described a highly diastereoselective synthesis of 2,5-disubstituted tetrahydrofurans (**2**) by Lewis acid catalyzed cycloaddition of donor-acceptor (D–A) cyclopropanes (**1**) and aldehydes (Scheme 1). Further, tetrahydrofuran **2** can undergo decarboxylation in a stereoselective manner to afford monoester **3** in good yield.[6] So, it should allow simple functionalization of the ring at the 3-position. This discovery is significant in synthetic organic chemistry because functionalized tetrahydrofurans occur in a variety of pharmacologically relevant natural products and the structures of tetrahydrofurans repetitively occur in natural products. In Pohlhaus' experiment,[7] by utilizing $Sn(OTf)_2$ (OTf = trifluoromethane sulfonate) as a catalyst and CH_2Cl_2 as a solvent, the cycloaddition reaction of D–A cyclopropanes [(*S*)-**1**] and benzaldehyde afforded tetrahydrofuran **2** in 96% *ee*, 100% conversion and >100:1 diastereomeric ratio. On the contrary, strong Lewis acids such as $TiCl_4$ and $AlCl_3$ give significant decomposition of the cyclopropane, whereas several milder Lewis acids such as $SnCl_2$, $ZnCl_2$, $Mg(OTf)_2$ and $La(OTf)_2$ exhibit no reactivity towards the cyclopropane. Interestingly, their labelling study in which one of the diastereotopic carboxymethyl groups of the cyclopropane was deuterated, compound **4**, and subjected to the normal reaction conditions revealed 94% of the label to be *cis* to the phenyl groups in the tetrahydrofuran.

In light of this, Pohlhaus et al. assumed this cycloaddition reaction was unlikely to proceed by S_E2 attack[8,9] or by a $[\pi 2_s + \sigma 2_a]$ mechanism,[10] but likely through an unusual initial S_N2 corner attack on the activated cyclopropane. In addition, they suggested that the ligand control might not be necessary. Considering this significant method for the preparation of regiodefined tetrahydrofurans, it was necessary to arbitrate the cycloaddition reaction mechanism to account for the specific function of the $Sn(OTf)_2$ in the activation of the D–A cyclopropanes. Hence, the comprehensive theoretical investigation of the complete reaction cycle for the $Sn(OTf)_2$-catalyzed synthesis of 2,5-disubstituted tetrahydrofuran from D–A cyclopropane and benzaldehyde was performed in the present work.

[a] School of Chemistry, Sichuan University,
Chengdu 610064, People's Republic of China
E-mail: zjs-xs@163.com
[b] School of Chemistry and Chemical Engineering, Southwest University,
Chongqing 400715, People's Republic of China
E-mail: liming@swu.edu.cn
Supporting information for this article is available on the WWW under http://www.eurjoc.org or from the author.

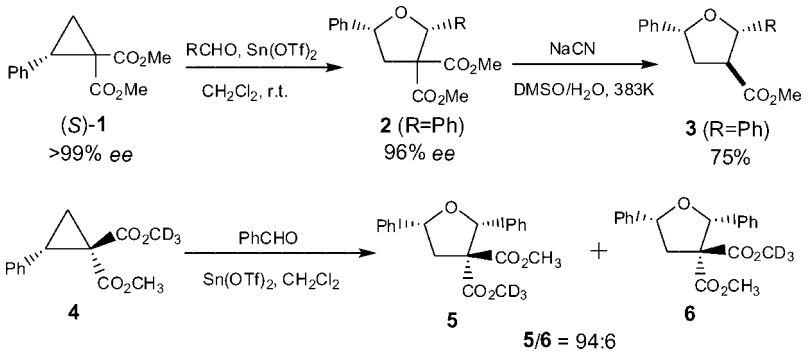

Scheme 1.

Computational Methods and Models

The present computations were based on the cycloaddition reaction of (*S*)-**1** with benzaldehyde catalyzed by $Sn(OTf)_2$. All computations were carried out by using the Gaussian03 program package.[11] Density functional theory (DFT) methods[12] have now been widely applied to various molecular systems with great success because of their efficiency and accuracy.[13–15] Especially the B3LYP method,[16,17] which includes Becke's three-parameter-exchange functionals and nonlocal Lee–Yang–Parr correlation functional that generally provide better results. In this paper, by taking into account the accuracy and the facility of the calculations, B3LYP/6-311G(*d,p*) (LANL2DZ adding one set of *d*-polarization function with exponent of 0.18[18] for Sn) single-point energies based on the B3LYP/6-31G (LANL2DZ basis set[19–21] for Sn) optimized structures were obtained. This strategy should be appropriate and feasible for this larger system (Figure S7 and Table S11). The transition states were verified by intrinsic reaction coordinate (IRC)[22] calculations and by animating the negative eigenvector coordinates with a visualization program (Molekel 4.3).[23,24] The intermediates were characterized by all real frequencies.

In addition, solvent effects of CH_2Cl_2 were studied by performing self-consistent reaction field (SCRF) single-point calculations by employing the polarizable continuum model (PCM)[25] approach based on the B3LYP/6-31G gas phase optimized geometry of each species at the B3LYP/6-311G(*d,p*) level. By utilizing Gibbs free energy including all electrostatic and nonelectrostatic terms, the reaction rate coefficients for key steps were computed by transition-state theory (TST).[26]

Furthermore, the bonding characteristics were analyzed by using the "atoms in molecules" (AIM) theory,[27] which is based on a topological analysis of the electron charge density and its Laplacian. The magnitude of the electron density, $\rho(r)$, at the bond critical points (BCPs) depends on the interatomic distance and the degree of coordination of

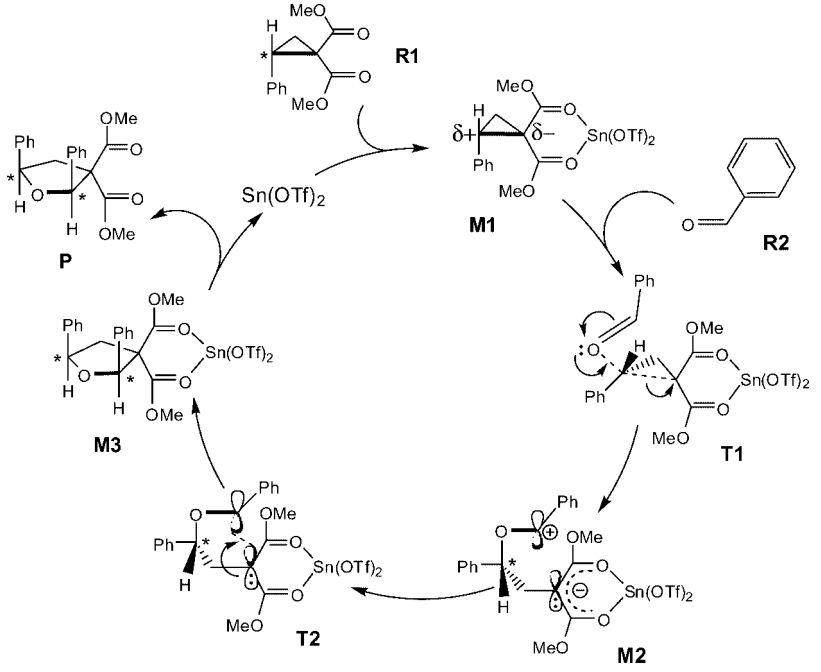

Scheme 2.

the atoms, and it is often used as a measure of the bond strength or similar type of bonds.[28] The analysis went further with those obtained by means of the natural bond orbital (NBO) theory.[29–32] AIM analysis was carried out by employing the AIM2000 code[33] with the B3LYP/6-31G wave functions as input. NBO analysis was performed by utilizing NBO5.0 code[34] with the optimized structures.

Results and Discussion

The complete reaction cycle for the $Sn(OTf)_2$-catalyzed synthesis of 2,5-disubstituted tetrahydrofuran by D–A cyclopropane (*S*)-**1** and benzaldehyde includes the following four steps: (1) D–A cyclopropane activation, (2) S_N2 attack at the carbon in the 2-position of the activated cyclopropane, (3) formation of the tetrahydrofuran coordination complex and (4) regeneration of the catalyst (Scheme 2). Ten possible reaction channels leading to *cis*-(2*R*,5*R*)-**P1**, *cis*-(2*S*,5*S*)-**P2** and *trans*-(2*R*,5*S*)-**P3** were located. Specially, unless otherwise specified, the B3LYP/6-311G(*d,p*)//B3LYP/6-31G energies including solvent effects were used in the following discussion.

CAT Coordination Reaction with R1

The Sn^{2+} ion has the $(5s)^2$ configuration; hence, a nonbonding electron pair can have a stereochemical influence. Thus, the structure of $Sn(\eta^2\text{-}OTf)_2$ shows tin with four oxy-

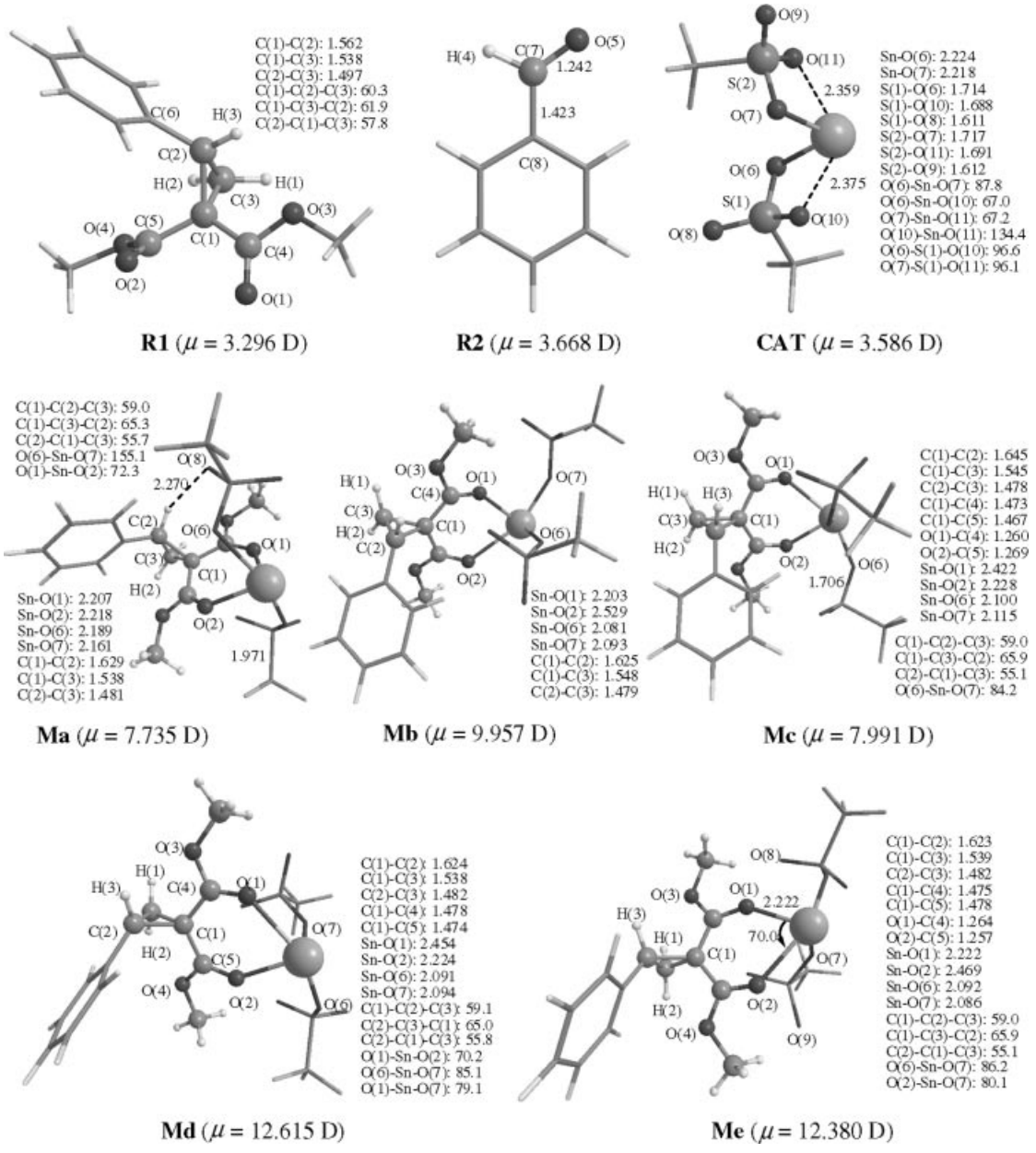

Figure 1. Geometries and parameters of the reactants, catalyst, and the five isomers of $Sn(\eta^1\text{-}OTf)_2(\eta^2\text{-}\mathbf{R1})$ (CF_3SO_3 and C_6H_5 are represented by sticks for clarity, bond lengths in Å, angles and dihedral angles in °, dipole moments, μ, in Debye).

gen neighbours on one side and a "vacant" coordination site apparently occupied by the lone pair of electrons (Figure S2). In addition, Sn–O(6) and Sn–O(7) are stronger than Sn–O(10) and Sn–O(11), because O(6) and O(7) are more negative than O(10) and O(11) in the atomic polar tensors (APT) charges (Table S4), and Sn–O(6) and Sn–O(7) are higher than Sn–O(10) and Sn–O(11) in the Wiberg bond orders. Because the carbonyl oxygen atoms of (*S*)-**1** (**R1**) have electron pairs in a p orbital, the coordination reaction between **R1** and the catalyst leads to the complex $Sn(\eta^1\text{-}OTf)_2(\eta^2\text{-}\mathbf{R1})$. However, whereas the two carbonyl oxygen atoms of **R1** are close to the Sn^{2+} ion, O(10) and O(11) leave it. Thus the Sn^{2+} ion keeps its four coordination in the $Sn(\eta^1\text{-}OTf)_2(\eta^2\text{-}\mathbf{R1})$. Five possible stereoisomers were located: **Ma**, **Mb**, **Mc**, **Md** and **Me** (Figure 1).

$Sn(\eta^1\text{-}OTf)_2(\eta^2\text{-}\mathbf{R1})$ differs from **R1** in electron structural characters. For **Ma**: (1) the NBO energy of the antibonding orbital $\sigma^*_{(C1–C2)}$ decreases by 251.3 kJ mol^{-1} (Table S2); (2) the positive APT charge at C(2) increases by 0.322, whereas the negative APT charges at C(1), O(1) and O(2) increase by –0.382, –0.264 and –0.310, respectively (Table S4); thus, the bonding dipole moment of $\sigma_{(C1–C2)}$ increases by 0.715 D; (3) the angular deviation of $\theta_{(C1–C2)}$ increases, whereas $\theta_{(C1–C3)}$ and $\theta_{(C2–C3)}$ decrease (Table S1); (4) the molecular orbital occupied electrons and electron density $\rho(r)$ at the BCP of $\sigma_{(C1–C2)}$ decrease, whereas the electron density $\rho(r)$ at the ring critical point (RCP) of the C(1)–C(2)–C(3) decreases remarkably. Evidently, the bent bond $\sigma_{(C1–C2)}$ of **Ma** becomes more unstable, and the carbon at the 2-positon exhibits electrophilic behaviour, whereas the carbon at the 1-positon exhibits nucleophilic behaviour.

Mb, **Mc**, **Md** and **Me** resemble **Ma** in electron structural characters (Table S1). Synoptically, $Sn(\eta^1\text{-}OTf)_2(\eta^2\text{-}\mathbf{R1})$ is much lower than **R1** in the NBO energy of the antibonding orbital $\sigma^*_{(C1–C2)}$. The lower the energy of the antibonding $\sigma^*_{(C1–C2)}$ orbital the easier it is for this orbital to accept electrons from an attacking nucleophile. In short, **R1** is remarkably activated by its combination with the catalyst. However, the difference in the stretching directions of the trifluoromethane sulfonates coordinated with Sn^{2+} leads to the remarkable differences in the dipole moments, solvent effects, steric hindrance effects and stereoelectronic effects. Therefore, the five stereoisomers of $Sn(\eta^1\text{-}OTf)_2(\eta^2\text{-}\mathbf{R1})$ exhibit very different activities in the further cycloaddition reactions with benzaldehyde.

Ma Reaction with R2

The initial nucleophilic substitution reaction of **Ma** occurs while the formyl oxygen attacks the carbon at the 2-position of the cyclopropane. Three possible reaction pathways, (1), (2) and (3), leading to products **P1a**, **P2** and **P3**, respectively, were located (Scheme 3).

In pathway (1), S_N2 corner attack at C(2) occurs, which leads to transition state **Ta1** (Figure 2). NBO analysis of **Ta1** indicates that C(1) and C(2) are sp^2 hybridized and that the dipole moments of $\sigma_{(C7–O5)}$ and $\sigma_{(C1–C2)}$ increase remarkably. This reveals the electron transfer from C(7) to O(5) and C(2) to C(1). The electron density increase in C(1) leads to a conjugated system O(1)–C(4)–C(1)–C(5)-O(2), which further strengthens the coordination forces of Sn–O(1) and Sn–O(2). Noticeably, the $H_{CHO}(4)\cdots O(8)$ distance of 2.424 Å is shorter than the standard H···O van der Waals distance of 2.720 Å (Bondi value);[35] hence, it is likely a hydrogen bond. Moreover, the angular deviations of $\theta_{(C1–C3)}$ and $\theta_{(C2–C3)}$ decrease to 7.1 and 11.8°, respectively. This reveals the remarkable elimination of bond strain in the cyclopropane. However, the high stabilization energy (obtained from the second-order perturbation analysis of donor–acceptor interactions in the NBO basis and used to estimate the strengths of the donor–acceptor interactions of the NBOs) of 205.2 kJ mol^{-1} for $(sp^{10.7})_{O5}\rightarrow(p)_{C2}$ reveals the electron transfer tendency from O(5) to C(2).

In the $\sigma_{(O5–C2)}$ bond formation process, as a result of the orientation effect of the $H_{CHO}(4)\cdots O(8)$ hydrogen bond, H(3)–C(2)–C(6) rotates along $\sigma_{(C2–C3)}$ in a clockwise manner. Ultimately, the H(3) and the phenyl of the cyclopropane overturn. Hence, the chiral carbon centre of C(2) becomes (*R*) configured. In **Ma1**, because of the APT charges –0.783 at C(1) and +1.124 at C(7), an intramolecular nucleophilic reaction can occur, which would lead to ring closure

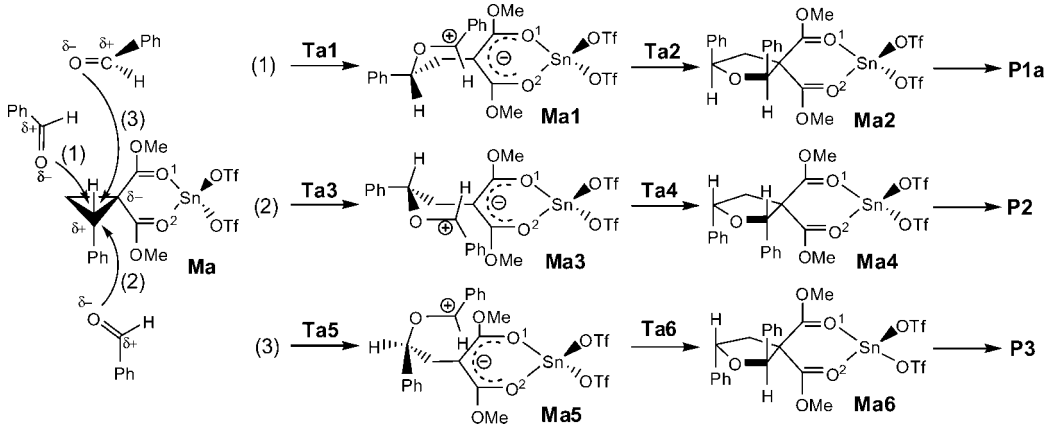

Scheme 3.

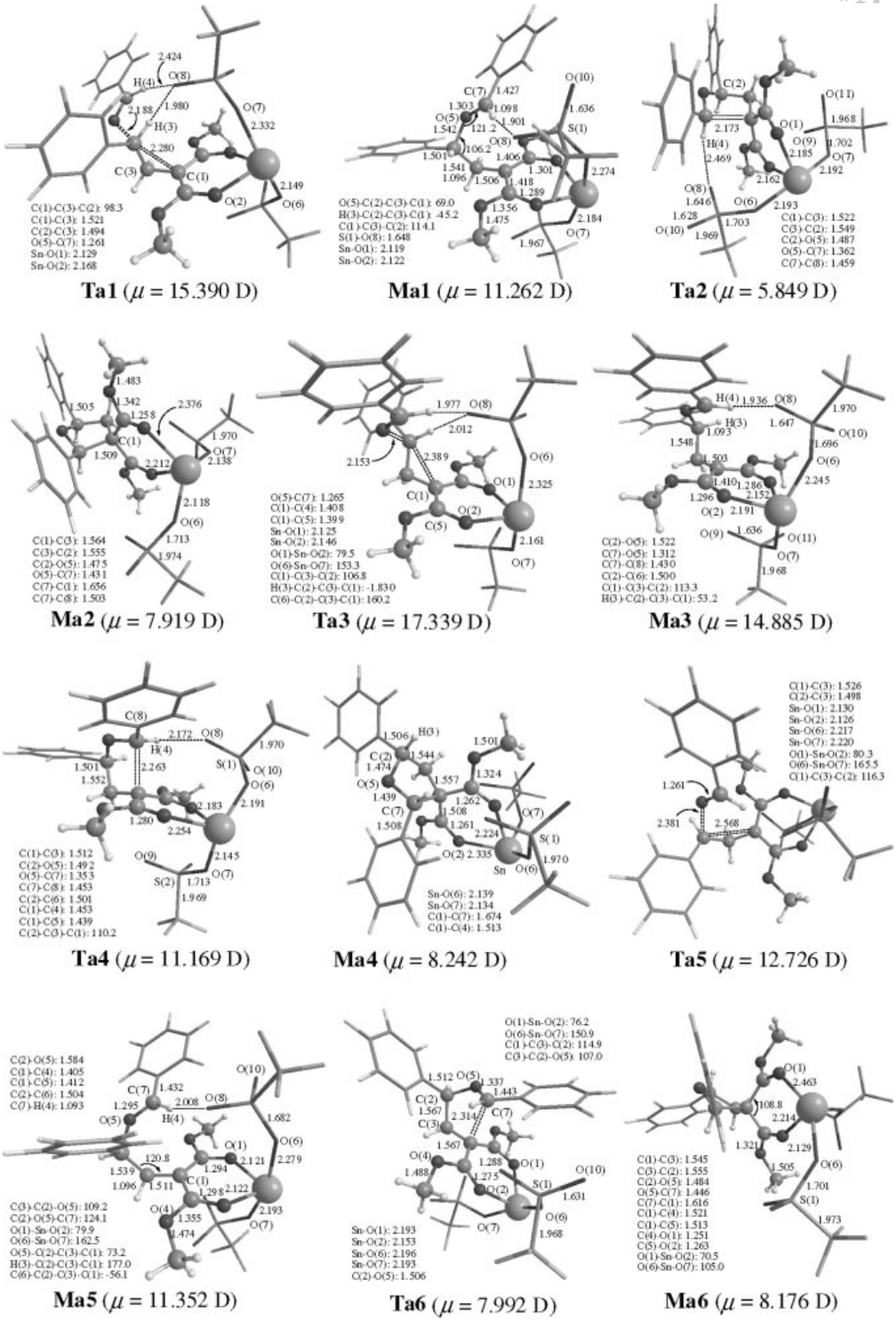

Figure 2. Geometries and parameters of the stationary points in the reactions of **Ma** with benzaldehyde **R2** (CF_3SO_3 and C_6H_5 are represented by sticks for clarity, bond lengths in Å, angles and dihedral angels in °, dipole moments, μ, in Debye).

via early tight transition state **Ta2** (Figure 2). Eventually, prochiral C(7) becomes a chiral carbon centre with the (*R*) configuration. Because C(1) is sp^3 hybridized, the conjugated system O(1)–C(4)–C(1)–C(5)–O(2) is destroyed; fur-

ther, Sn–O(1) and Sn–O(2) are weakened. Finally, **Ma2** dissociates into *cis*-(2*R*,5*R*)-tetrahydrofuran [**P1a**, corresponding to **5**, its two phenyls are *cis* to O(1)].

In pathway (2), the formyl oxygen attacks C(2) from the bottom right corner. As a result of steric repulsion between the phenyl and trifluoromethane sulfonate groups, H(3)–C(2)–C(6) rotates along $\sigma_{(C2-C3)}$ in a clockwise manner. In **Ta3** (Figure 2), there is evidence for $H_{CHO}(4)\cdots O(8)$, and C(1) is sp^2 hybridized. The rich p electrons of C(1) leads to a conjugated system O(1)–C(4)–C(1)–C(5)–O(2), which further enhances the coordination strength of Sn–O(1) and Sn–O(2). In addition, the high stabilization energy of 240.4 kJ mol^{-1} for $(sp^{9.29})_{O5}\rightarrow(p)_{C2}$ reveals the p electron transfer tendency from O(5) to C(2).

In **Ma3**, $H_{CHO}(4)\cdots O(8)$ becomes stronger, and C(2) keeps the (*S*) chiral configuration. C(1) and C(7) are sp^2 hybridized and exhibit high negative (–0.781) and positive (1.250) APT charges, respectively. So, an intramolecular nucleophilic reaction can occur, which would lead to ring closure with a very low barrier energy (Table 1 and Figure 3). However, $H_{CHO}(4)\cdots O(8)$ is weak in **Ta4** and **Ma4** (Figure 2). Finally, **Ma4** dissociates into *cis*-(2*S*,5*S*)-**P2** and the catalyst.

In pathway (3), the nucleophilic reaction goes through formyl oxygen attack at C(2) from the top right corner. Because of the steric repulsion between the phenyl and trifluoromethane sulfonate groups as the formyl oxygen approaches C(2), the angels O(1)–Sn–O(6) and O(6)–Sn–O(7) increase. A hydrogen bond $H_{CHO}(4)\cdots O(8)$ exists in **Ta5** and **Ma5** (Figure 2), and it can control the stretching direction of benzaldehyde. As the intramolecular nucleophilic reaction proceeds further, **Ma5** transforms into **Ma6**, which can further dissociate into *trans*-(2*R*,5*S*)-**P3** and the catalyst.

As shown in Table 1 and Figure 3, each of the **Ma** reaction pathways include two nucleophilic reactions, and the first one, which suffers from a much higher energy barrier, is rate controlling. Both in the gas phase and in the absence of CH_2Cl_2, pathway (1) is absolutely favoured, and *cis*-(2*R*,5*R*)-**P1a** is the dominant product.

Table 1. The reaction barriers for the entropy $\Delta S^{\neq}$ (J mol^{-1} K^{-1}), energy $\Delta E^{\neq}$ (kJ mol^{-1}) and Gibbs free energy $\Delta G^{\neq}$ (kJ mol^{-1}) of the transition states.

Transition states	In gas phase			In CH_2Cl_2	
	$\Delta S^{\neq}$[a]	$\Delta G^{\neq}$[a]	$\Delta E^{\neq}$[b]	$\Delta G^{\neq}$[a]	$\Delta G^{\neq}$[b]
Ta1	–144.1	54.6	18.5	25.7	42.7
Ta2	–28.0	26.4	13.9	33.8	28.6
Ta3	–163.5	59.5	39.9	22.7	60.9
Ta4	–38.5	14.6	1.5	16.6	11.4
Ta5	–175.8	85.8	57.5	52.6	85.2
Ta6	–16.7	26.3	19.2	24.6	21.5
Tb1	–194.6	62.3	36.7	28.5	69.4
Tc1	–196.7	61.2	26.4	31.1	64.6
Tb2	–5.6	30.0	9.0	40.0	13.1
Td1	–175.1	86.6	55.6	50.7	81.2
Td2	–19.3	28.9	6.2	20.3	3.0
Td3	–163.7	92.1	68.5	43.1	73.9
Te1	–174.5	92.4	64.8	31.4	64.4
Te2	–14.7	34.7	15.1	32.9	15.9
Te3	–154.9	108.3	85.6	59.3	89.9
Te4	–39.8	0.7	0.6	33.8	23.3
Te5	–153.4	108.5	85.1	57.3	86.1

[a] Obtained from B3LYP/6-31G calculations. [b] Obtained from B3LYP/6-311G(*d,p*)//B3LYP/6-31 calculations.

Mb and Mc Reactions with R2

Akin to pathway (1), the **Mb** and **Mc** reactions [pathways (4) and (5), respectively] proceed by initial S_N2 attack at the carbon in the 2-positon of the cyclopropane, which leads to the same intermediate **Mb1** and the product **P1a** (Scheme 4).

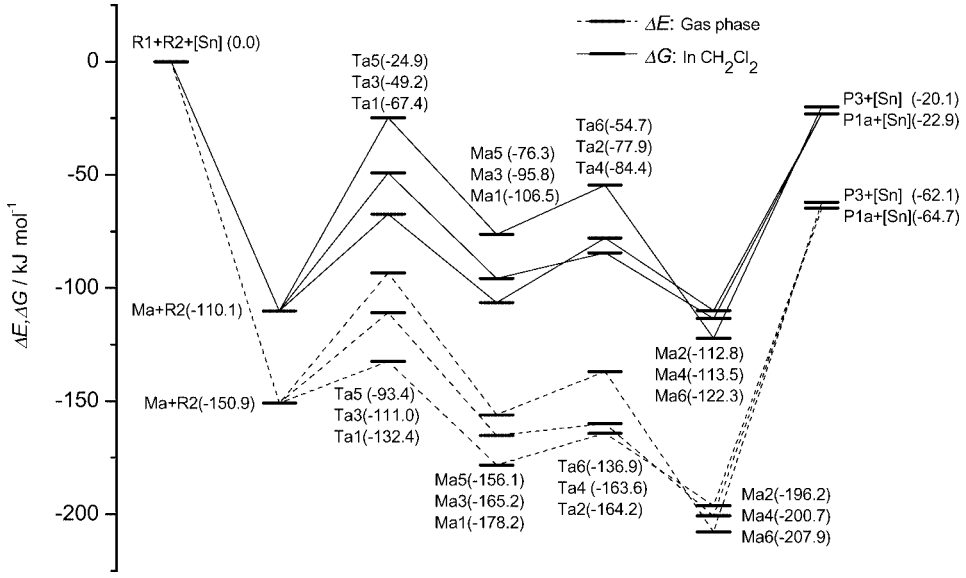

Figure 3. The schematic reaction profiles of **Ma** with benzaldehyde [dash lines represent the relative energies ΔE in the gas phase, solid lines represent the relative Gibbs free energies ΔG; solvation energies, which were obtained from B3LYP/6-311g(*d,p*)//B3LYP/6-31G calculations, are included].

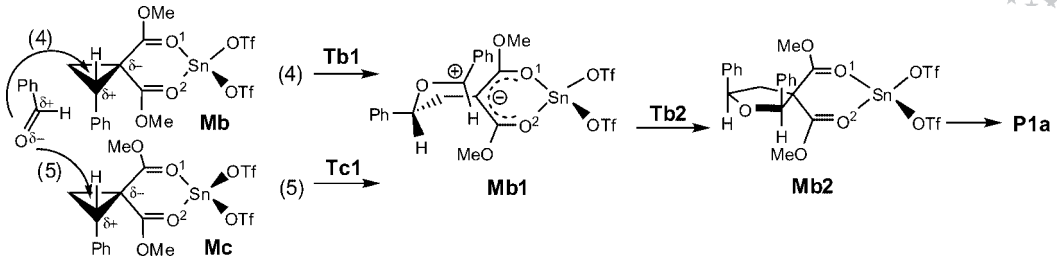

Scheme 4.

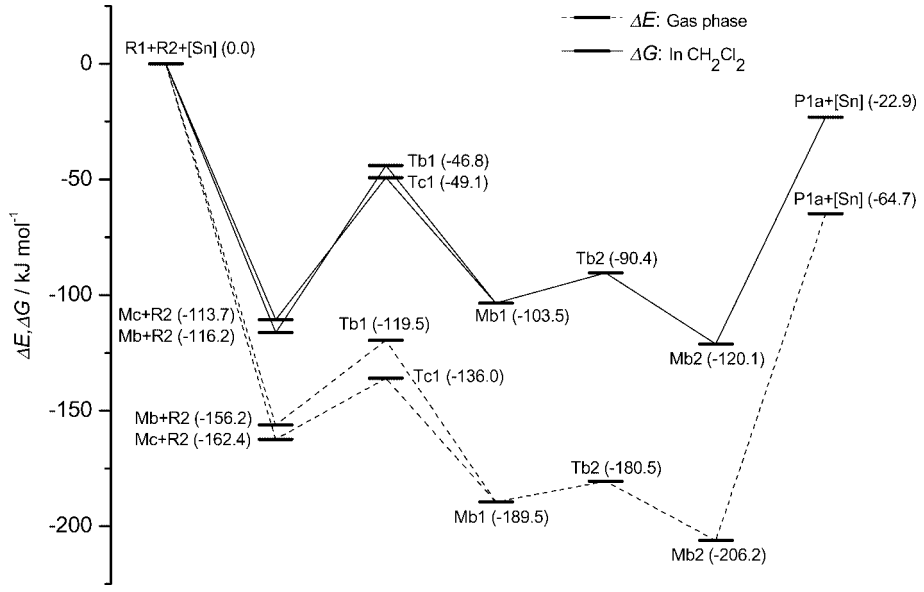

Figure 4. The schematic reaction profiles of **Mb** and **Mc** with benzaldehyde [dash lines represent the relative energies ΔE in the gas phase, solid lines represent the relative Gibbs free energies ΔG; solvation energies, which were obtained from B3LYP/6-311g(*d,p*)//B3LYP/6-31G calculations, are included].

In the **Mb1** formation process, because of the $H_{CHO}(4)\cdots O$ interaction, H(3)–C(2)–C(6) rotates along σ_{C2-C3}, H(3) and the phenyl group turn upside down and benzaldehyde moves to the right of C(2). Hence, C(2) adopts the (*R*) chiral configuration. Further, an intramolecular nucleophilic reaction occurs, which leads to ring closure with a very low energy barrier. Finally, **Mb2** dissociates into *cis*-(2*R*,5*R*)-**P1a**.

As shown in Table 1 and Figure 4, both in the gas phase and in CH_2Cl_2, the S_N2 reaction is the rate-determining step.

Md Reaction with R2

There are two alternative routes at the initial stage of the **Md** pathway: through **Td1** and **Td3** [pathways (6) and (7), respectively] with barrier heights of 81.2 and 73.9 kJ mol^{-1}, respectively (Scheme 5). In **Td1** and **Td3**, both the increases in the negative APT charges at C(1) and O(5) and the positive APT charges at C(2) and C(7) reveal the electronic transfer from $\sigma_{(O5-C7)}$ to $p_{(O5)}$ and from $\sigma_{(C1-C2)}$ to $p_{(C1)}$. In addition, a conjugated system O(1)–C(4)–C(1)–C(5)–O(2) strengthens the Sn^{2+} coordination force with O(1) and O(2). Noticeably, in the transformation process of **Td1** to **Md1**, as a result of the $H_{CHO}(4)\cdots O(9)$ interaction and the steric hindrance effect of the trifluoromethane sulfonate and methoxy groups, C(3) overturns to the another side of C(1)–C(2) (Figure S4); thus, C(2) becomes (*R*) configured. Further, an intramolecular nucleophilic reaction occurs between C(1) and C(7) with a remarkably low energy barrier of 3.0 kJ mol^{-1}, which leads to ring close product **Md2**. Ultimately, **Md2** dissociates into *cis*-(*R*,*R*)-tetrahydrofuran [**P1b**, corresponding to **6**. Unlike **P1a**, the two phenyls of **P1b** are *trans* to O(1)] and the catalyst.

However, in the forward direction of transition state **Td3**, unexpectedly, only the ring-closed coordination complex **Md3** was located, and our numerous attempts to locate other stationary points between **Td3** and **Md3** failed. By analyzing the structure of **Td3** or by animating the negative eigenvector coordinates with a visualization program, it is affirmed that **Md** + **R2**→**Md3** is unlikely a $[_{\pi}2_s + _{\sigma}2_a]$ mechanism.[10] Also, by comparison with the energy gaps of interacting NBOs, the $[_{\pi}2_s + _{\sigma}2_a]$ mechanism is the most unfavourable (Tables S2 and S3). However, it can be explained that a possible intermediate **M2** positioned in the forward direction of transition state **Td3** is too unstable to

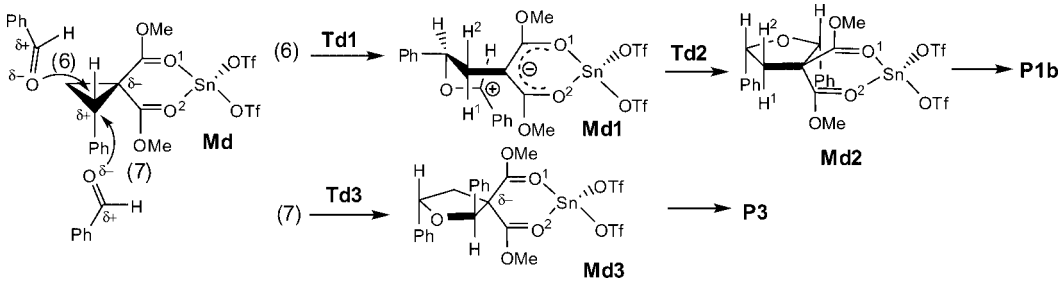

Scheme 5.

Table 2. The reaction rate coefficients of the selected reactions at 298.15K in CH_2Cl_2.

Entry	Reactions	k_2 / $dm^3 mol^{-1} s^{-1}$	Reactions	k_3 / s^{-1}	Reactions	k_{M2} / $dm^6 mol^{-2} s^{-1}$
1	**Ma** + **R2**→**Ma1**	5.02×10^{6}	**Ma1**→**Ma2**	6.09×10^{7}	**R1** + **R2** + **CAT**→**Ma1**	6.39×10^{23}
2	**Ma** + **R2**→**Ma3**	3.25×10^{3}	**Ma3**→**Ma4**	6.24×10^{10}	**R1** + **R2** + **CAT**→**Ma3**	4.22×10^{20}
3	**Ma** + **R2**→**Ma5**	1.80×10^{-1}	**Ma5**→**Ma6**	1.04×10^{9}	**R1** + **R2** + **CAT**→**Ma5**	2.32×10^{16}
4	**Mb** + **R2**→**Mb1**	1.05×10^{2}	**Mb1**→**Mb2**	3.09×10^{10}	**R1** + **R2** + **CAT**→**Mb1**	1.59×10^{20}
5	**Mc** + **R2**→**Mb1**	7.30×10^{2}	–	–	**R1** + **R2** + **CAT**→**Mb1**	4.11×10^{20}
6	**Md** + **R2**→**Md1**	9.02×10^{-1}	**Md1**→**Md2**	1.82×10^{12}	**R1** + **R2** + **CAT**→**Md1**	9.15×10^{18}
7	**Md** + **R2**→**Md3**	1.71×10	–	–	**R1** + **R2** + **CAT**→**Md3**	1.70×10^{20}
8	**Me** + **R2**→**Me1**	7.92×10^{2}	**Me1**→**Me2**	1.03×10^{10}	**R1** + **R2** + **CAT**→**Me1**	9.85×10^{21}
9	**Me** + **R2**→**Me3**	2.70×10^{-2}	**Me3**→**Me4**	5.22×10^{8}	**R1** + **R2** + **CAT**→**Me3**	3.30×10^{17}
10	**Me** + **R2**→**Me5**	1.25×10^{-1}	–	–	**R1** + **R2** + **CAT**→**Me5**	1.55×10^{18}

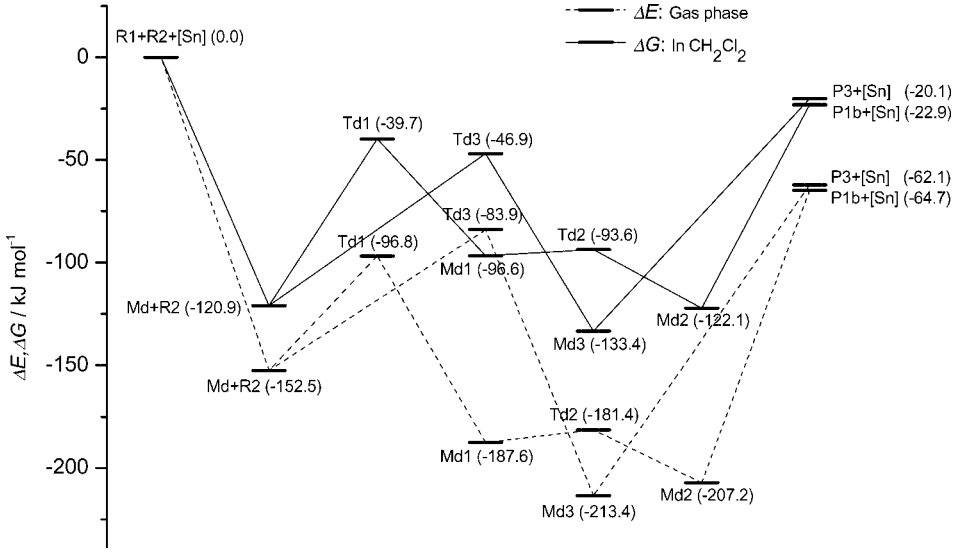

Figure 5. The schematic reaction profiles of **Md** with benzaldehyde [dash lines represent the relative energies ΔE in the gas phase, solid lines represent the relative Gibbs free energies ΔG; solvation energies, which were obtained from B3LYP/6-311G(*d,p*)//B3LYP/6-31G calculations, are included].

be located. Just as mentioned above, the intramolecular nucleophilic reactions of **M2**→**M3** easily occur between C(1) (with high negative APT charge) and C(7) (with high positive APT charge) because it suffers from a remarkably low energy barrier. Most importantly, pathway (7) is very unfavourable (Tables 1 and 2) in the (*S*)-**1** reactions. So we did not pay further attention to this. Finally, **Md3** associates into *trans*-(2*R*,5*S*)-**P3**.

As Figure 5 shows, in the gas phase, **Td1** is lower in energy by 12.9 kJ mol^{-1} than **Td3** in the forward reaction energy barrier, whereas in the absence of the CH_2Cl_2 solvent, **Td1** is higher by 7.3 kJ mol^{-1} than **Td3**. This indicates that the solvent effect cannot to be ignored in the **Md** reactions.

Me Reaction with R2

Me reactions go through pathways (8), (9) and (10), which leads to **P1b**, **P3** and **P2**, respectively (Scheme 6).

Akin to pathway (6), reaction pathway (8) is initiated by an S_N2 corner attack on the activated cyclopropane. Similarly, because of steric hindrance between the phenyl and

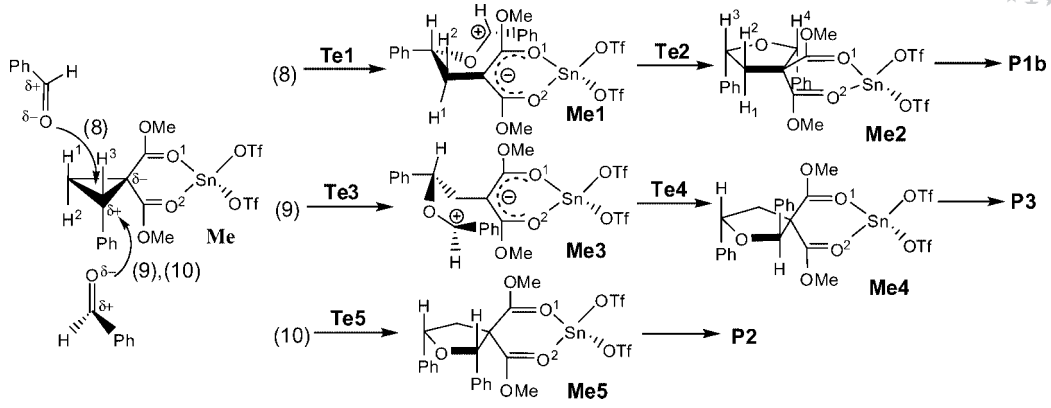

Scheme 6.

methoxy groups in the $\sigma_{(C2–O5)}$ formation process, $\sigma_{(C3–C1)}$ rotates in an anticlockwise manner and C(3) overturns to the another side of the $\sigma_{(C1–C2)}$ bond. In **Te1** and **Me1**, there is evidence for a $H_{CHO}(4)\cdots O(8)$ bond, and C(1) and C(7) exhibit high negative and positive APT charges, respectively. Hence, the intramolecular nucleophilic reaction of **Me1**→**Me2** goes smoothly by suffering from a very low energy barrier of 15.9 kJ mol^{-1}. Ultimately, **Me2** decomposes into **P1b** and the catalyst.

Both pathways (9) and (10) go through formyl oxygen attack at C(2) from the bottom right corner. They are different in the H(4) stretching directions and the phenyl group positions. In **Te3**, H(4) points downward and the benzaldehyde plane is nearly vertical to the C(1)–C(2)–C(3) plane and parallel to the C(4)–C(1)–C(5) plane. In **Te5**, H(4) points rightward and benzaldehyde is nearly coplanar with the C(1)–C(2)–C(3) plane and vertical to the C(4)–C(1)–C(5) plane.

In **Me3**, C(2) keeps the (*S*) chiral configuration. Further internal nucleophilic reaction leads to ring closure and the chiral carbon centre C(7) with (*R*) configuration. Finally, **Me4** dissociates into the catalyst and **P3**.

Akin to reaction pathway (7), in the forward reaction to transition state **Te5** of pathway (10) only the ring closing **Me5** was located. By analyzing the structure of **Te5** or by animating the negative eigenvector coordinates with a visualization program, it is affirmed that **Me** + **R2**→**Me5** is unlikely a concerted asynchronous cycloaddition. In the same way, it can be explained as the former expression. Ultimately, **Me5** releases the catalyst and yields *cis*-(2*S*,5*S*)-**P2**.

As Figure 6 shows, the reactions of **Me** experience high energy barriers, especially reaction pathways (9) and (10). So the **Me** reaction pathways are reduced to absolute inferiority in the (*S*)-**1** reactions (see Table 2).

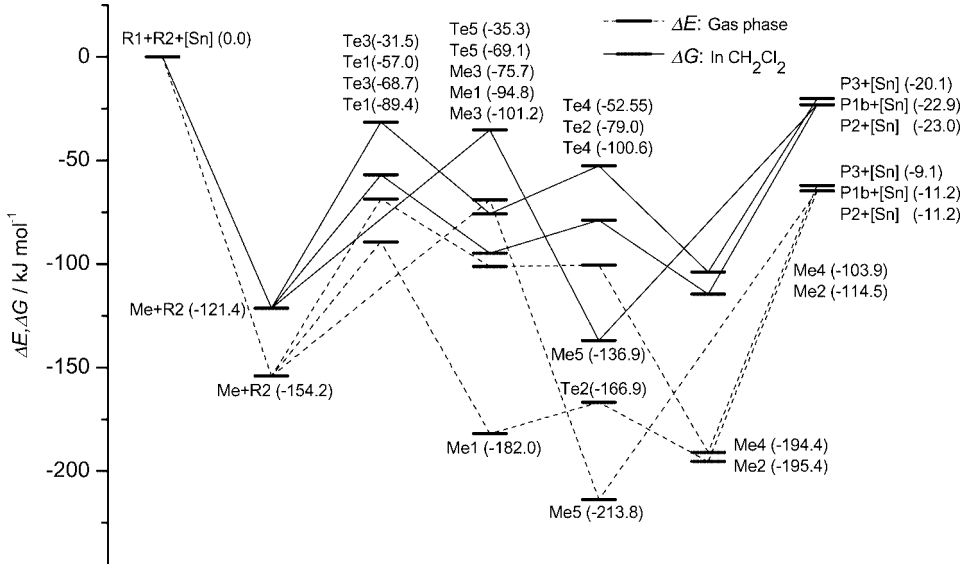

Figure 6. The schematic reaction profiles of **Me** with benzaldehyde [dash lines represent the relative energies Δ*E* in the gas phase, solid lines represent the relative Gibbs free energies Δ*G*; solvation energies, which were obtained from B3LYP/6-311g(*d,p*)//B3LYP/6-31G calculations, are included].

Rate Coefficients and Reaction Ratios

As described above, the overall reaction cycle includes four elementary reactions generally:

(a) $\mathbf{R1} + \mathbf{CAT} \xrightarrow{k_1} \mathbf{M1}$

(b) $\mathbf{M1} + \mathbf{R2} \xrightarrow{k_2} \mathbf{M2}$

(c) $\mathbf{M2} \xrightarrow{k_3} \mathbf{M3}$

(d) $\mathbf{M3} \xrightarrow{k_4} \mathbf{P} + \mathbf{CAT}$

where k_1, k_2, k_3 and k_4 are the forward rate coefficients. Reaction (a) occurs with very negative Gibbs free energy changes (–110.1 to –120.9 kJ mol^{-1}), whereas reactions (b) and (c) proceed via **T1** and **T2**, respectively, and **T2** is remarkably lower in energy than **T1** in the forward reaction energy barriers. So, reaction (b) is the bottleneck in the process of generating chiral product **M3**. Therefore, k_3 will not appear in the overall rate expression for the formation of **M3**.

According to transition state theory, the elementary reaction rate coefficient of reaction (b) can be obtained by:

$$k_2 = \frac{k_B T}{h} (p^\theta)^{\Delta n^\neq} \exp\left(-\frac{\Delta G_1^\neq (p^\theta)}{RT}\right)$$

where the $\Delta G_1^\neq(p^\theta)$ is the Gibbs free energy barrier of **T1**, k_B is the Boltzmann's constant, h is Planck's constant and T is the absolute temperature.

By using the prior equilibria state approximation method[36,37] and by taking into account the equilibrium constant, the rate of formation of **M2** can be provided by:

$$\frac{d[\mathbf{M2}]}{dt} = k_2 \times K_1 [\mathbf{R1}][\mathbf{CAT}] \times [\mathbf{R2}]$$
$$= k_{\mathbf{M2}} \times [\mathbf{R1}][\mathbf{R2}][\mathbf{CAT}]$$

where $k_{\mathbf{M2}}$ is the overall reaction rate coefficient for the formation of **M2** and K_1 is the equilibrium constant of reaction (a). This equation reveals that the overall reaction for the formation of **M2** is third-order. However, the concentration of catalyst is generally kept as a constant and thus the observed kinetics becomes second-order. The calculated reaction rate coefficients are listed in Table 2.

According to the reaction rate coefficients, reaction pathways (1), (2), (3), (4), (5), (6), (7), (8), (9) and (10) account for 98.3, 6.5×10^{-2}, 3.6×10^{-6}, 2.5×10^{-2}, 6.3×10^{-2}, 1.4×10^{-3}, 2.6×10^{-2}, 1.5, 5.1×10^{-5} and 2.4×10^{-4}%, respectively, and the product ratios can be obtained: **P1** = 99.9 % (in which **P1a/P1b**, 98:2, compared with the experimental data of 94:6[6]), **P2** = 0.07 % and **P3** = 0.03 %.

Overview of the Mechanism

As described above, the key in the enantiospecific synthesis of disubstituted tetrahydrofuran that was developed by Pohlhaus et al. is the activation of D–A cyclopropane and the two nucleophilic reactions. Obviously, an essential requirement for the activation of the D–A cyclopropane is the decrease in the NBO energy of the antibonding $\sigma^*_{(C1-C2)}$ orbital, which is caused by the Lewis acid Sn(OTf)$_2$ coordination reaction. As shown in Figure 7, in benzaldehyde the p-LP$_{(O5)}$ is higher 281.2 kJ mol^{-1} than $\pi_{(C7-O5)}$ in NBO energy. By comparison with the energy gaps of interacting NBOs, the S_N2 mechanism is the most reasonable (except with the use of the catalyst). On the contrary, the [$_\pi2_s$ + $_\sigma2_a$] mechanism is the most unfavourable (Tables S2 and S3).

Theoretically, in an S_N2 mechanism, the substrate is favoured to be attacked by a nucleophile from the side opposite the leaving group and front approach is disfavoured because the σ* orbital is less in the region between the carbon atom and the leaving group and because the front-side approach would involve both a bonding and an antibonding interaction with the σ* orbital as it has a nodal surface between the atoms. These can satisfactorily account for why the reaction of (*S*)-**1** with benzaldehyde yields *cis*-(2*R*,5*R*)-

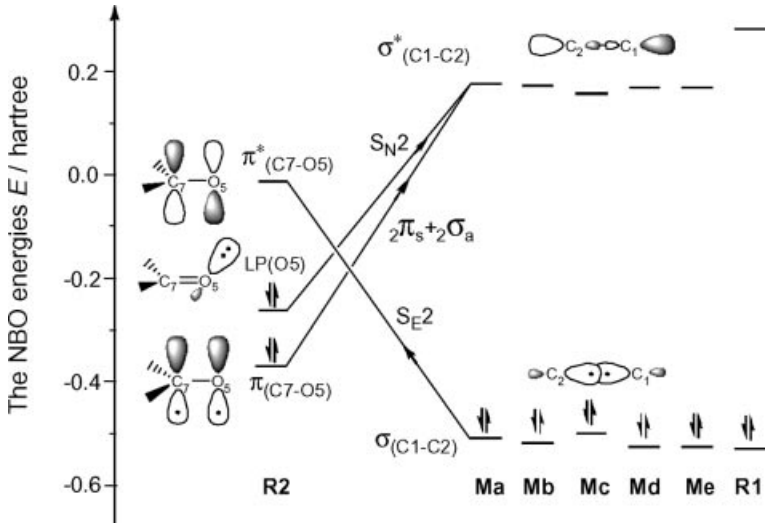

Figure 7. The NBO interactions of benzaldehyde and the D–A cyclopropanes in the different mechanisms.

P1 dominantly, and why all the reaction pathways leading to **P1** are instigated by formyl oxygen attack at the carbon of the 2-position by $Sn(\eta^1\text{-}OTf)_2(\eta^2\text{-}\mathbf{R1})$ from the top left corner.

With regard to the solvent effects of CH_2Cl_2, nearly all the solvation energies (ΔG^{sol}) of the stationary points (except for the reactants, catalyst, **Me3**, **Td3**, **Te1**, **Te3** and **Te5**) are positive and likely appear negative relative to the molecular dipole moments. On the whole, the solvent effects make the reaction energy barriers increase. As one trifluoromethane sulfonate group can generate a hydrogen bond $H_{CHO}(4)\cdots O_{(OTf)}$ to control the aldehyde stretching directions in the S_N2 reactions (a steric help effect), and its direction heavily influences the activity of $Sn(\eta^1\text{-}OTf)_2(\eta^2\text{-}\mathbf{R1})$ (steric hindrance and stereoelectronic effects), the function of the trifluoromethane sulfonate group appears significant.

Conclusions

The $Sn(OTf)_2$-catalyzed synthesis of disubstituted tetrahydrofurans from D–A cyclopropane and benzaldehyde includes four elementary reactions: (1) activation of the D–A cyclopropane; (2) S_N2 attack on the activated D–A cyclopropane; (3) ring close reaction; (4) regeneration of the catalyst. In the D–A cyclopropane activation reaction, the NBO energy of $\sigma^*_{(C1–C2)}$ decreases remarkably and the dipole moment of $\sigma_{(C1–C2)}$ increases. The two chiral carbon centres of tetrahydrofuran are generated in the second and third steps. The second is rate-controlling. The solvent effects of CH_2Cl_2 cause the reaction energy barriers to increase. The ligand of the trifluoromethane sulfonate group can generate a hydrogen bond of $H_{CHO}(4)\cdots O_{(OTf)}$ to control the stretching directions of benzaldehyde. Reasonably, the *cis*-(2*R*,5*R*)-tetrahydrofuran is the predicted dominant product, and the most favoured reaction channel is **R1 + R2 + CAT → Ma + R2 → Ma1 → Ma2 → P1a**.

Supporting Information (see footnote on the first page of this article): Computational details about the geometries, bond characters, electrostatic pictures, APT and NBO charges of the stationary points in the reactions.

Acknowledgments

J. Z. thanks Prof. Tian An-Ming at Sichuan University of China for his valuable suggestions. This work was supported by the Key Project of Science and Technology of the Ministry of Education, P. R. (grant No. 104263), Natural Science Foundation of Chongqing City, P. R. (grant No. CSTC-2004BA4024).

[1] Y. Sugita, K. Kawai, I. Yokoe, *Heterocycles* **2001**, *55*, 135–144.
[2] Z. Han, S. Uehira, T. Tsuritani, H. Shinokubo, K. Oshima, *Tetrahedron* **2001**, *57*, 987–995.
[3] H. U. Reissig, H. Holzinger, G. Glomsda, *Tetrahedron* **1989**, *45*, 3139–3150.
[4] M. P. Sibi, Z. Ma, C. P. Jasperse, *J. Am. Chem. Soc.* **2005**, *127*, 5764–5765.
[5] I. S. Young, M. A. Kerr, *Angew. Chem. Int. Ed.* **2003**, *42*, 3023–3026.
[6] P. D. Pohlhaus, J. S. Johnson, *J. Am. Chem. Soc.* **2005**, *127*, 16014–16015.
[7] P. D. Pohlhaus, J. S. Johnson, *J. Org. Chem.* **2005**, *70*, 1057–1059.
[8] J. M. Coxon, P. J. Steel, B. I. Whittington, *J. Am. Chem. Soc.* **1988**, *110*, 2988–2990.
[9] H. U. Reissig, H. Holzinger, G. Glomsda, *Tetrahedron* **1989**, *45*, 3139–3150.
[10] P. G. Wiering, J. W. Verhoeven, H. Steinberg, *J. Am. Chem. Soc.* **1981**, *103*, 7675–7676.
[11] M. J. Frisch, G. W. Trucks, H. B. Schlegel, G. E. Scuseria, M. A. Robb, J. R. Cheeseman, J. A. Montgomery, J. T. Vreven, K. N. Kudin, J. C. Burant, J. M. Millam, S. S. Iyengar, J. Tomasi, V. Barone, B. Mennucci, M. Cossi, G. Scalmani, N. Rega, G. A. Petersson, H. Nakatsuji, M. Hada, M. Ehara, K. Toyota, R. Fukuda, J. Hasegawa, M. Ishida, T. Nakajima, Y. Honda, O. Kitao, H. Nakai, M. Klene, X. Li, J. E. Knox, H. P. Hratchian, J. B. Cross, C. Adamo, J. Jaramillo, R. Gomperts, R. E. Stratmann, O. Yazyev, A. J. Austin, R. Cammi, C. Pomelli, J. W. Ochterski, P. Y. Ayala, K. Morokuma, G. A. Voth, P. Salvador, J. J. Dannenberg, V. G. Zakrzewski, S. Dapprich, A. D. Daniels, M. C. Strain, O. Farkas, D. K. Malick, A. D. Rabuck, K. Raghavachari, J. B. Foresman, J. V. Ortiz, Q. Cui, A. G. Baboul, S. Clifford, J. Cioslowski, B. B. Stefanov, G. Liu, A. Liashenko, P. Piskorz, I. Komaromi, R. L. Martin, D. J. Fox, T. Keith, M. A. Al-Laham, C. Y. Peng, A. Nanayakkara, M. Challacombe, P. M. W. Gill, B. Johnson, W. Chen, M. W. Wong, C. Gonzalez, A. Pople, *Gaussian 03*, Revision B.03, Gaussian, Pittsburgh, PA, **2003**.
[12] R. G. Parr, W. Yang, *Density-Functional Theory of Atoms and Molecules*, Oxford University Press, New York, **1989**.
[13] L. Pisano, M. Farriol, X. Asensio, I. Gallardo, A. González-Lefont, J. M. Lluch, J. Marquet, *J. Am. Chem. Soc.* **2002**, *124*, 4708–4715.
[14] A. B. Pierini, D. M. A. Vera, *J. Org. Chem.* **2003**, *68*, 9191–9199.
[15] D. A. Pratt, M. L. Heer, P. Mulder, K. U. Ingold, *J. Am. Chem. Soc.* **2001**, *123*, 5518–5526.
[16] A. D. Becke, *J. Chem. Phys.* **1993**, *98*, 5648–5652.
[17] C. Lee, W. Yang, R. G. Parr, *Phys. Rev. B* **1988**, *37*, 785–789.
[18] A. W. Ehlers, M. Böhme, S. Dapprich, A. Gobbi, A. Höllwarth, V. J. K. F. Könler, R. Stegmann, A. Veldkamp, G. A. Frenking, *Chem. Phys. Lett.* **1993**, *208*, 237–240.
[19] P. J. Hay, W. R. Wadt, *J. Chem. Phys.* **1985**, *82*, 270–283.
[20] W. R. Wadt, P. J. Hay, *J. Chem. Phys.* **1985**, *82*, 284–297.
[21] P. J. Hay, W. R. Wadt, *J. Chem. Phys.* **1985**, *82*, 299–310.
[22] C. Gonzalez, H. B. J. Schlegel, *Phys. Chem.* **1990**, *94*, 5523–5527.
[23] P. Flükiger, H. P. Lüthi, S. Portmann, J. Weber, *MOLEKEL 4.3*, Swiss Center for Scientific Computing, Manno, Switzerland, **2000**–**2002**.
[24] S. Portmann, H. P. Lüthi, *Chimia* **2000**, *54*, 766–770.
[25] S. Miertus, J. Tomasi, *Chem. Phys.* **1982**, *65*, 239–245.
[26] H. Eyring, H. Gershinowitz, C. E. San, *J. Chem. Phys.* **1935**, *3*, 786–796.
[27] R. F. W. Bader, *International Series of Monographs in Chemistry Vol. 22: Atoms in Molecules – A Quantum Theory*, Oxford University Press, Oxford, U. K., **1990**.
[28] R. F. W. Bader, P. L. A. Popelier, T. A. Keith, *Angew. Chem. Int. Ed. Engl.* **1994**, *33*, 620–631.
[29] J. E. Carpenter, F. J. Weinhold, *Mol. Struct. (THEOCHEM)* **1988**, *169*, 41–50.
[30] A. E. Reed, L. A. Curtiss, F. Weinhold, *Chem. Rev.* **1988**, *88*, 899–926.
[31] J. P. Foster, F. Weinhold, *J. Am. Chem. Soc.* **1980**, *102*, 7211–7218.
[32] A. E. Reed, R. B. Weinstock, F. J. Weinhold, *J. Chem. Phys.* **1985**, *83*, 735–746.

[33] F. Biegler-König, J. Schönbohm, R. Derdau, D. Bayles, R. F. W. Bader, *AIM 2000, Version 2.0*, McMaster University, **2002**.
[34] E. D. Glendening, J. K. Badenhoop, A. E. Reed, J. E. Carpenter, J. A. Bohmann, C. M. Morales, F. Weinhold, *NBO 5.0*, Theoretical Chemistry Institute, University of Wisconsin, Madison, WI, **2001**.
[35] A. Bondi, *J. Phys. Chem.* **1966**, *70*, 3006–3007.
[36] Y. Y. Wei, J. Li, *The Conspectus of Chemical Reaction Mechanism*, 1st ed., Beijing, Science Press, **2004**, pp. 58.
[37] X. S. Zhao, *The Conspectus of Chemical Reaction Theory*, 1st ed., Beijing, Peking University Press, **2003**, pp. 6.
Received: March 12, 2007
Published Online: July 30, 2007

